Commun Nonlinear Sci Numer Simulat 85 (2020) 105221

Contents lists available at ScienceDirect

Commun Nonlinear Sci Numer Simulat

journal homepage: www.elsevier.com/locate/cnsns

Research paper

An improved car-following model accounting for the time-delayed velocity difference and backward looking effect

Guangyi Ma[a], Minghui Ma[a,*], Shidong Liang[b], Yansong Wang[a], Yaozong Zhang[a]

[a] School of Mechanical and Automotive Engineering, Shanghai University of Engineering Science, 201620 Shanghai, China
[b] Business School, University of Shanghai for Science and Technology, Shanghai 200093, China

ARTICLE INFO

Article history:
Received 21 October 2019
Revised 17 January 2020
Accepted 5 February 2020
Available online 6 February 2020

Keywords:
Car-following model
Traffic flow
Time-delayed velocity difference
TDGL equation

ABSTRACT

In order to explore the impacts of the time-delayed velocity difference and backward looking effect on traffic flow, this paper proposes an improved car-following model based on the full velocity difference model (FVDM) by accounting for the time-delayed velocity difference and backward looking effect. The linear stability condition of the proposed model is derived by taking advantage of the linear stability theory. The time-dependent Ginzburg-Landau (TDGL) equation and the modified Korteweg-de Vries (mKdV) equation are established based on the nonlinear theory to describe the evolution of the traffic density waves near the critical stability point. Moreover, the link between the TDGL and mKdV equations is also provided. Finally, the results from both the numerical simulation and the theoretical analysis show that the proposed model can not only strengthen the stability of traffic flow, but also suppress the traffic congestion.

1. Introduction

With the rapid development of social economy, the speed of construction of road facilities is far less than the rate of increase of vehicles, which leads to the worsening of traffic conditions, and brings a series of traffic problems such as traffic jam, traffic safety and so on. In addition, with the increase of vehicle density, the characteristics of vehicle interaction become more and more obvious. Drivers need to pay attention to more and more information, arousing considerable concerns from many aspects [1–3]. Considering the above situation, many traffic models have been proposed to analyze traffic behavior and interpret complex traffic phenomena, which mainly include car-following models [4–7], cellular automation models [8,9], continuum models [10,11] and lattice hydrodynamic models [12,13].

The optimal velocity model (OVM), proposed by Bando et al. [14] in 1995, is a classic car-following model to describe the actual traffic flow phenomena, such as the spread of traffic jams, stop and go. In order to solve the problems of very high acceleration and unreasonable deceleration, drawbacks exhibited by the OVM, in 1998, Helbing and Tilch [15] developed a generalized force model (GFM) by accounting for the negative velocity difference based on the OVM. The GFM takes into account only the influence of the negative velocity difference to the current car, which is a problem that, in 2001, Jiang et al. [16] solved, by proposing the full velocity difference model (FVDM), where the positive velocity difference is considered, based on the GFM. In 2012, Sun et al. [17] presented the backward looking and velocity difference (BLVD) model by introducing the backward looking effect on the basis of the FVDM. According to the above analysis, the performance of

* Corresponding author.
E-mail addresses: maminghui1989@hotmail.com (M. Ma), jzwbt@163.com (Y. Wang).

https://doi.org/10.1016/j.cnsns.2020.105221
1007-5704/

the models proves to be constantly improving. In the actual driving process of the vehicle, the driver will adjust the velocity difference with the preceding vehicle in real time, in order to maintain the optimal velocity. At the same time, to ensure safe driving, the driver will also observe the rear vehicle's situation through the rear-view mirror of the vehicle.

There are a lot of nonlinear phenomena in actual traffic system, and traffic jam is the most typical nonlinear phenomenon in traffic flow. In recent years, many researchers study the traffic jam by using the nonlinear analysis. Komastu and Sasa [18] derived the mKdV equation to investigate the long time behavior near a critical point and describe traffic jams. Nagatani [19] derived the TDGL equation from the car-following model to describe traffic jams as kink-antikink density waves. Peng et al. [20] estimated the impact of optimal velocity changes with memory on jam transition by deriving the mKdV equation. Chen et al. [21] obtained the kink-antikink solution of the TDGL equation and the mKdV equation from an improved car-following model in Intelligent Transportation System. Song et al. [22] derived the TDGL equation and the mKdV equation, they showed that traffic jams can be described by the kink-antikink solution of the TDGL equation and the mKdV equation. According to different equation parameters and initial conditions, different equations and their corresponding solutions can be obtained [23]. Li et al. [24] derived the Burgers equation, Korteweg-de Vries (KdV) equation and mKdV equation respectively in stable, metastable and unstable regions in terms of equation parameters and initial conditions. Nagatani [25] found that triangular shock wave, soliton wave and kink-antikink wave appear respectively in the three regions of traffic flow, which are described by the Burgers, KdV and mKdV equations. Zhou et al. [26] studied the traffic wave of the optimal velocity difference model and described traffic jams by using the Burgers, KdV and mKdV equations.

As early as in 1958, time delay was recognized as an important influencing parameter in traffic research [27]. It is mainly derived from the time required by the driver from perceiving the changes in the surrounding environment to acting accordingly, while it is mainly influenced by the driver's own condition and the surrounding environment. Time delay might have an important effect on traffic flow characteristics. Therefore, it is necessary to conduct more in-depth research on time delay in traffic flow. Davis [28] studied the effects of time delay due to driver reaction times through simulations and analysis of the OVM of traffic dynamics. Orosz et al. [29,30] discussed the local and global bifurcations of the OVM which features the reactive time delay of drivers, while Yu et al. [31] researched the density waves of the OVM. Zhou et al. [32] studied the density waves of the optimal velocity difference model (OVDM), featuring the reaction-time delay of drivers. Zhang et al. [33] considered the effect of the time-delayed velocity difference on vehicle acceleration due to reactive time delayed effect of drivers.

To sum up, these models can describe the phase transition of traffic flow and interpret some actual traffic phenomena. However, these models are unsuitable for modeling the time-delayed velocity difference and backward looking effect, because they do not consider these two factors simultaneously. Actually, the time-delayed velocity difference and backward looking effect, both reflect every driver's conditions. It takes a period of time for drivers to switch from perceiving the surrounding environment to acting accordingly. Meanwhile, in order to maintain safe driving, the driver also views the condition of the rear vehicle from the rear-view mirror of the vehicle. By considering the time-delayed velocity difference and backward looking effect simultaneously, not only the results are closer to the actual traffic, but also the stability of traffic flow can be enhanced. In light of the aforementioned points, the proposed car-following model is presented based on the FVDM by taking into account the impacts of the time-delayed velocity difference and backward looking effect on traffic flow in this paper. For reasons of convenience, the proposed model is abbreviated as the TVBL model.

The contributions of this paper are:

(1) The problem of how to better describe traffic behavior and avoid the traffic jams under the vehicles interact environment is solved by proposing an improved car-following model. Some previous studies have considered the time-delayed velocity difference and backward looking effect separately. However, they have never considered the above two factors simultaneously. In this paper, an improved car-following model considering the impacts of the time-delayed velocity difference and backward looking effect on traffic flow is proposed. Considering more information, the evolution of traffic flow and the mechanism of vehicle movement under the increasingly obvious vehicle interaction can be better described.
(2) The theoretical analysis is applied to analyze the performance of the extended car-following model. Through linear and nonlinear analysis, the performance of the improved model is much better than that of the previous models which consider the time-delayed velocity difference and backward looking effect separately. Simulation is used to verify the accuracy of the theoretical analysis. The simulation shows that not only the results are closer to the actual traffic flow, but also the stability of traffic flow can be enhanced. The simulation results are in accordance with the conclusions of the theoretical analysis.

The remainder of the paper is organized as follows. In Section 2, a modified car-following model is put forward, considering the time-delayed velocity difference and backward looking effect. In Section 3, the stability analysis is presented, based on the linear stability theory. In Section 4, the nonlinear stability analysis near the critical stability point for the TVBL model is carried out, and the TDGL equation is derived. In Section 5, the mKdV equation is obtained. In Section 6, numerical simulation is carried out to verify the results of the theoretical analysis, while the complete study is summarized in Section 7.

2. Model

The optimal velocity model (OVM), proposed by Bando et al. [14] in 1995, is a classic car-following model, to describe the actual traffic flow phenomena, such as the spread of traffic jams, stop and go. The dynamic Eq. (1) is shown.

$$\frac{dv_n(t)}{dt} = \alpha[V(\Delta x_n(t)) - v_n(t)] \tag{1}$$

where α is the sensitivity coefficient of the driver's distance, $v_n(t)$ is the velocity of car n at time t, $\Delta x_n(t) = x_{n+1}(t) - x_n(t)$ is the distance difference between the $(n+1)$th and the nth vehicles at time t, $V(\Delta x_n(t))$ is the optimal velocity function.

In order to solve the problems of very high acceleration and unreasonable deceleration, drawbacks exhibited by the OVM, in 1998, Helbing and Tilch [15] developed a generalized force model (GFM) by accounting for the negative velocity difference based on the OVM. The respective dynamic Eq. (2) is given.

$$\frac{dv_n(t)}{dt} = \alpha[V(\Delta x_n(t)) - v_n(t)] + \lambda H(-\Delta v_n(t))\Delta v_n(t) \tag{2}$$

where H is the Heaviside function, λ is different from the sensitivity coefficient of α, $\Delta v_n(t) = v_{n+1}(t) - v_n(t)$ is the velocity difference between the $(n+1)$th and the nth vehicles at time t.

The GFM takes into account only the influence of the negative velocity difference to the current car, which is a problem that, in 2001, Jiang et al. [16] solved, by proposing the full velocity difference model (FVDM), where the positive velocity difference is considered, based on the GFM. The model Eq. (3) is given.

$$\frac{dv_n(t)}{dt} = \alpha[V(\Delta x_n(t)) - v_n(t)] + k\Delta v_n(t) \tag{3}$$

where $k = \lambda\alpha$ is the sensitivity coefficient of the relative velocity.

In 2012, Sun et al. [17] presented the backward looking and velocity difference (BLVD) model by introducing the backward looking effect on the basis of the FVDM. The dynamic Eq. (4) is shown.

$$\frac{dv_n(t)}{dt} = \alpha[pV_F(\Delta x_n(t)) + (1-p)V_B(\Delta x_{n-1}(t)) - v_n(t)] + k\Delta v_n(t) \tag{4}$$

where $\Delta x_{n-1}(t) = x_n(t) - x_{n-1}(t)$ is the distance difference between car n and car $n-1$ at time t, p represents the relative roles of the two optimal velocity functions, $V_F(\Delta x_n(t))$ and $V_B(\Delta x_{n-1}(t))$ are the optimal velocity functions for forward and backward observations, respectively.

Based on the FVDM and considering the complexity of the actual traffic, it takes few time for drivers to respond to the current traffic circumstances. At the same time, in order to drive safely, the driver also observes the rear vehicle's state through the rear-view mirror of the vehicle. In light of the aforementioned facts, a modified car-following model is proposed considering the time-delayed velocity difference and backward looking effect, which can be formulated in Eq. (5).

$$\frac{dv_n(t)}{dt} = \alpha[pV_F(\Delta x_n(t)) + (1-p)V_B(\Delta x_{n-1}(t)) - v_n(t)] + k\Delta v_n(t) + r[v_n(t) - v_n(t-t_d)] \tag{5}$$

where t_d is the reaction-time delay of drivers, assuming that all drivers have the same reaction-time delay, α is the sensitivity coefficient corresponding to the inverse of the delay time τ, $v_n(t) - v_n(t-t_d)$ represents the velocity difference of car n between time t and time $t-t_d$ due to reactive time t_d delayed effect, r is the sensitivity coefficient of the time-delayed velocity difference $v_n(t) - v_n(t-t_d)$, and the optimal velocity functions are proposed in Eqs. (6) and (7).

$$V_F(\Delta x_n(t)) = \alpha'[\tanh(\Delta x_n(t) - h_c) + \tanh(h_c)] \tag{6}$$

$$V_B(\Delta x_{n-1}(t)) = -\alpha''[\tanh(\Delta x_{n-1}(t) - h_c) + \tanh(h_c)] \tag{7}$$

where α', α'' are positive constants. The function V_F has a turning point $\Delta x_n = h_c : V_F''(h_c) = 0$ and the function V_B has also a turning point $\Delta x_{n-1} = h_c : V_B''(h_c) = 0$. When $p \neq 1$ and $r = 0$, the TVBL model just considers the influences of the front vehicle's state and backward looking effect on the current car, hence the BLVD model is derived. When $p = 1$ and $r = 0$, the TVBL model becomes the FVDM, while it does not consider the influences of the time-delayed velocity difference and backward looking effect on the current car.

3. Linear stability analysis

Linear stability analysis methodology is applied to study the performance of the TVBL model under small perturbations. Assuming the initial state of traffic flow is stable, and all vehicles are uniformly distributed with the uniform headway h and the corresponding optimal speed $pV_F(h) + (1-p)V_B(h)$. Therefore, the vehicle's position of the steady traffic flow is:

$$x_n^0(t) = hn + (pV_F(h) + (1-p)V_B(h))t, h = L/N \tag{8}$$

where L is the length of the road and N is the total number of vehicles.

Let $y_n(t) = e^{(ikn+zt)}$ be a small deviation from the traffic flow steady state $x_n^0(t)$:

$$x_n(t) = x_n^0(t) + y_n(t) \tag{9}$$

Substituting Eq. (9) into Eq. (5) and linearizing the derived equation, the result is shown in Eq. (10).

$$\frac{d^2y_n(t)}{dt^2} = \alpha\left[pV_F'(h)\Delta y_n + (1-p)V_B'(h)\Delta y_{n-1} - \frac{dy_n(t)}{dt}\right] + k\frac{d\Delta y_n(t)}{dt} + r\left[\frac{dy_n(t)}{dt} - \frac{dy_n(t-t_d)}{dt}\right] \tag{10}$$

where $V_F'(h) = dV_F(\Delta x_n)/d\Delta x_n|\Delta x_n = h$, $V_B'(h) = dV_B(\Delta x_{n-1})/\Delta x_{n-1}|\Delta x_{n-1} = h$, $\Delta y_n(t) = y_{n+1}(t) - y_n(t)$ and $\Delta y_{n-1}(t) = y_n(t) - y_{n-1}(t)$.

According to the Fourier series, Expanding $y_n(t)$ in Eq. (10), it derives:

$$z^2 = \alpha\left[pV_F'(h)\left(e^{ik}-1\right) + (1-p)V_B'(h)\left(1-e^{-ik}\right) - z\right] + kz\left(e^{ik}-1\right) + rt_dz^2 \tag{11}$$

Let $z = z_1(ik) + z_2(ik)^2 + \cdots$ and $e^{ik} = 1 + ik + \frac{1}{2}(ik)^2 + \cdots$, substituting these into Eq. (11) leads to the first- and the second-order terms of ik, respectively:

$$z_1 = pV_F'(h) + (1-p)V_B'(h) \tag{12}$$

$$z_2 = \frac{p}{2}V_F'(h) - \frac{1-p}{2}V_B'(h) - (1-rt_d)\tau z_1^2 + \lambda z_1 \tag{13}$$

The neutral stability condition is given in Eq. (14).

$$\tau = \frac{pV_F'(h) - (1-p)V_B'(h) + 2\lambda\left[pV_F'(h) + (1-p)V_B'(h)\right]}{2(1-rt_d)\left[pV_F'(h) + (1-p)V_B'(h)\right]^2} \tag{14}$$

The uniform traffic flow stable region is expressed in Eq. (15).

$$\tau < \frac{pV_F'(h) - (1-p)V_B'(h) + 2\lambda\left[pV_F'(h) + (1-p)V_B'(h)\right]}{2(1-rt_d)\left[pV_F'(h) + (1-p)V_B'(h)\right]^2} \tag{15}$$

When $p \neq 1$ and $r = 0$, the stability condition of the BLVD model is obtained in Eq. (16).

$$\tau < \frac{pV_F'(h) - (1-p)V_B'(h) + 2\lambda\left[pV_F'(h) + (1-p)V_B'(h)\right]}{2\left[pV_F'(h) + (1-p)V_B'(h)\right]^2} \tag{16}$$

When $p = 1$ and $r = 0$, Eq. (15) is transformed into the stability condition of the FVDM in Eq. (17).

$$\tau < \frac{1+2\lambda}{2V_F'(h)} \tag{17}$$

Fig. 1 shows the phase space (h, α) diagram of the FVDM with $p = 1$ and $r = 0$ s^{-1}, the BLVD model with $p = 0.9$ and $r = 0$ s^{-1}, the TVBL model with $p = 0.9$ and $r = 0.1$ s^{-1}, and the TVBL model with $p = 0.9$ and $r = 0.2$ s^{-1}, respectively. Other parameters are $\alpha' = 1$ m/s, $\alpha'' = 1$ m/s, $h_c = 4$ m, $\lambda = 0.2$, $t_d = 1$ s. The solid lines show the neutral stability curves of the above models, the coexistence lines obtained from the mKdV equation are indicated by the dotted lines. It can be clearly seen from Fig. 1 that the phase diagram is divided into three regions: the stable region which is above the coexistence line, the metastable region which is between the coexistence line and the neutral stability curve, and the unstable region which is below the neutral stability curve. In addition, every curve has a critical point, as r increases or p decreases, the position of critical point and critical stability curve is lowered, and the corresponding stable region expands. This means that the stability of traffic flow is enhanced, as the r value rises or the p value decreases. The stability region of the BLVD model is larger than that of the FVDM, which indicates that backward looking effect plays a role in improving the stability of traffic flow. However, the stability region of the TVBL model is larger than that of the BLVD model, which indicates that the TVBL model in this paper has a significant effect on enhancing the stability of traffic flow.

4. TDGL equation

In order to analyze the nonlinear dynamic characteristics of the TVBL model, the nonlinear wave equation is inferred, where the propagation characteristics of traffic congestion are demonstrated. In terms of coarse-grained scales, the long wave-length model is used to describe the traffic flow and the solution of the equation is obtained. The slow-varying characteristic of long waves near the critical stability point is analyzed. For reasons of convenience, Eq. (5) can be rewritten in light of the headway, as:

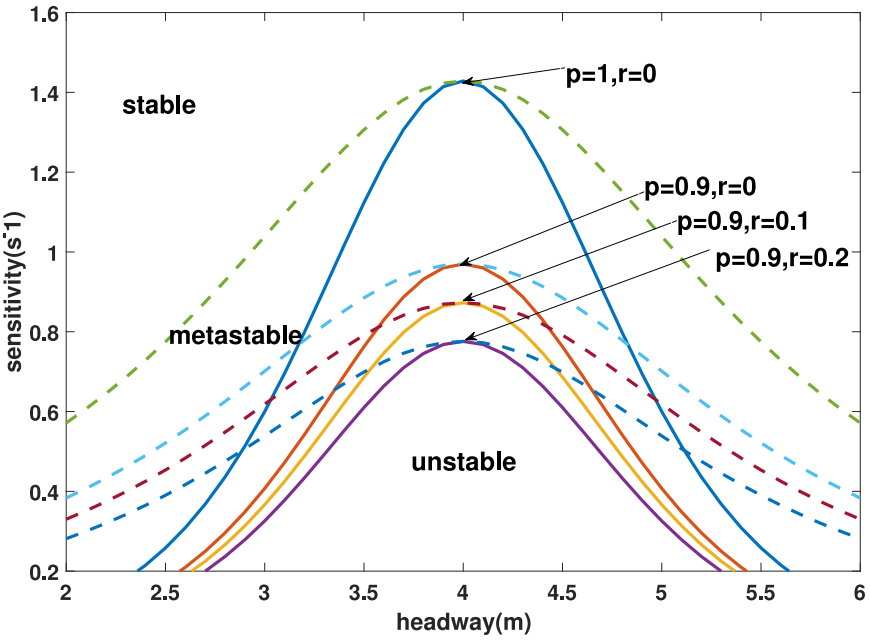

Fig. 1. The critical stability curves in the headway-sensitivity space.

$$\frac{d^2\Delta x_n(t)}{dt^2} = \alpha[p(V_F(\Delta x_{n+1}) - V_F(\Delta x_n)) + (1-p)(V_B(\Delta x_n) - V_B(\Delta x_{n-1}))] - \alpha\frac{d\Delta x_n(t)}{dt} + \lambda\alpha\left(\frac{d\Delta x_{n+1}(t)}{dt} - \frac{d\Delta x_n(t)}{dt}\right) + r\left[\frac{d\Delta x_n(t)}{dt} - \frac{d\Delta x_n(t-t_d)}{dt}\right] \tag{18}$$

The low scales for space variable n and time variable t are introduced, and the slow variable X and T are defined in Eq. (19) [22,24].

$$X = \varepsilon(n + bt), T = \varepsilon^3 t, 0 < \varepsilon \leq 1 \tag{19}$$

where b is the undetermined constant. The headway $\Delta x_n(t)$ is defined in Eq. (20).

$$\Delta x_n(t) = h_c + \varepsilon R(X, T) \tag{20}$$

Substituting Eqs. (19) and (20) into Eq. (18) and expanding Eq. (18) by using Taylor's formula to the fifth-order of ε, the nonlinear partial differential equation is obtained as:

$$\begin{aligned}
&\varepsilon^2\left[b - pV_F' - (1-p)V_B'\right]\partial_X R + \varepsilon^3\left(b^2\tau - \frac{1}{2}pV_F' + \frac{1-p}{2}V_B' - \lambda b - r\tau b^2 t_d\right)\partial_X^2 R \\
&+ \varepsilon^4\left\{\partial_T R - \left[\frac{1}{6}\left(pV_F' + (1-p)V_B'\right) + \frac{1}{2}\lambda b - \frac{1}{2}b^3 t_d^2 r\tau\right]\partial_X^3 R - \frac{1}{6}\left(pV_F''' + (1-p)V_B'''\right)\partial_X R^3\right\} \\
&+ \varepsilon^5\left\{(2b\tau - \lambda - 2bt_d r\tau)\partial_X\partial_T R - \left[\frac{1}{24}\left(pV_F' - (1-p)V_B'\right) + \frac{1}{6}\lambda b + \frac{1}{6}b^4 t_d^3 r\tau\right]\partial_X^4 R\right\} \\
&- \frac{1}{12}\varepsilon^5\left(pV_F''' - (1-p)V_B'''\right)\partial_X^2 R^3 = 0
\end{aligned} \tag{21}$$

where $V_F' = V_F'(h_c) = dV_F(\Delta x_n)/d\Delta x_n|\Delta x_n = h_c$, $V_B' = V_B'(h_c) = dV_B(\Delta x_{n-1})/d\Delta x_{n-1}|\Delta x_{n-1} = h_c$, $V_B''' = V_B'''(h_c) = d^3V_B(\Delta x_{n-1})/d\Delta x_{n-1}^3|\Delta x_{n-1} = h_c$ and $V_F''' = V_F'''(h_c) = d^3V_F(\Delta x_n)/d\Delta x_n^3|\Delta x_n = h_c$.

Following, the traffic flow near critical point $\tau = (1+\varepsilon^2)\tau_c$ is investigated. By taking $b = pV_F' + (1-p)V_B'$, the second-order and third-order terms of ε are eliminated from Eq. (21), which leads to the following equation.

$$\begin{aligned}
\varepsilon^4\partial_T R = {}& \varepsilon^4\left[\frac{1}{6}\left(pV_F' + (1-p)V_B'\right) + \frac{1}{2}\lambda b - \frac{1}{2}b^3 t_d^2 r\tau\right]\partial_X^3 R \\
&- \frac{\varepsilon^4}{6}\left(pV_F''' + (1-p)V_B'''\right)\partial_X R^3 + \varepsilon^3\left(-b^2\tau + \frac{1}{2}pV_F' - \frac{1-p}{2}V_B' + \lambda b + r\tau b^2 t_d\right)\partial_X^2 R \\
&- \varepsilon^5\left[\frac{1}{6}(2b\tau - \lambda - 2bt_d r\tau)\left(pV_F' + (1-p)V_B' + 3\lambda b - 3b^3 t_d^2 r\tau\right)\right]\partial_X^4 R
\end{aligned}$$

$$+\frac{1}{24}\varepsilon^5\left(pV_F'-(1-p)V_B'+4\lambda b+4b^4t_d^3r\tau\right)\partial_X^4R$$
$$+\varepsilon^5\left[\frac{1}{6}(2b\tau-\lambda-2bt_dr\tau)\left(pV_F'''+(1-p)V_B'''\right)-\frac{1}{12}\left(pV_F'''-(1-p)V_B'''\right)\right]\partial_X^2R^3 \tag{22}$$

By using $x=\varepsilon^{-1}X$ and $t=\varepsilon^{-3}T$, variable X and T in Eq. (22) are converted, and taking $S(x,t)=\varepsilon R(X,T)$, Eq. (22) is rewritten as Eq. (23).

$$\begin{aligned}\partial_tS=&\left[\frac{1}{6}\left(pV_F'+(1-p)V_B'\right)+\frac{1}{2}\lambda b-\frac{1}{2}b^3t_d^2r\tau\right]\partial_x^3S\\&-\frac{1}{6}\left(pV_F'''+(1-p)V_B'''\right)\partial_x^3S+\left[-b^2\tau+\frac{1}{2}pV_F'-\frac{1-p}{2}V_B'+\lambda b+r\tau b^2t_d\right]\partial_x^2S\\&-\left[\frac{1}{6}(2b\tau-\lambda-2bt_dr\tau)\left(pV_F'+(1-p)V_B'+3\lambda b-3b^3t_d^2r\tau\right)\right]\partial_x^4S\\&+\left[\frac{1}{24}\left(pV_F'-(1-p)V_B'+4\lambda b+4b^4t_d^3r\tau\right)\right]\partial_x^4S+\left[\frac{1}{6}(2b\tau-\lambda-2bt_dr\tau)\left(pV_F'''+(1-p)V_B'''\right)\right]\partial_x^2S^3\\&-\frac{1}{12}\left[pV_F'''-(1-p)V_B'''\right]\partial_x^2S^3\end{aligned} \tag{23}$$

By adding term $\frac{2(1-rt_d)\left[pV_F'+(1-p)V_B'\right]^2}{pV_F'-(1-p)V_B'+2\lambda\left[pV_F'+(1-p)V_B'\right]}\left[-b^2\tau+\frac{1}{2}pV_F'-\frac{1-p}{2}V_B'+\lambda b+r\tau b^2t_d\right]\partial_xS$ on both left and right sides of Eq. (23) and performing $t_1=t$ and $x_1=x-\frac{2(1-rt_d)\left[pV_F'+(1-p)V_B'\right]^2}{pV_F'-(1-p)V_B'+2\lambda\left[pV_F'+(1-p)V_B'\right]}\left[-b^2\tau+\frac{1}{2}pV_F'-\frac{1-p}{2}V_B'+\lambda b+r\tau b^2t_d\right]t$ for Eq. (23), the following equation is given:

$$\begin{aligned}.\partial_{t1}S=&\left\{\partial_{x1}-\frac{pV_F'-(1-p)V_B'+2\lambda\left[pV_F'+(1-p)V_B'\right]}{2(1-rt_d)\left[pV_F'+(1-p)V_B'\right]^2}\partial_{x1}^2\right\}\\&\times\left\{\left[\frac{1}{6}\left(pV_F'+(1-p)V_B'\right)+\frac{1}{2}\lambda b-\frac{1}{2}b^3t_d^2r\tau\right]\partial_x^3S-\frac{2(1-rt_d)\left[pV_F'+(1-p)V_B'\right]^2}{pV_F'-(1-p)V_B'+2\lambda\left[pV_F'+(1-p)V_B'\right]}\right.\\&\left.\times\left(-b^2\tau+\frac{1}{2}pV_F'-\frac{1-p}{2}V_B'+\lambda b+r\tau b^2t_d\right)S-\frac{1}{6}\left(pV_F'''+(1-p)V_B'''\right)S^3\right\}\end{aligned} \tag{24}$$

The thermodynamic potentials are defined as:

$$\begin{aligned}\phi(S)=&-\frac{2(1-rt_d)\left[pV_F'+(1-p)V_B'\right]^2}{pV_F'-(1-p)V_B'+2\lambda\left[pV_F'+(1-p)V_B'\right]}\left(-b^2\tau+\frac{1}{2}pV_F'-\frac{1-p}{2}V_B'+\lambda b+r\tau b^2t_d\right)S^2\\&+\frac{1}{24}\left[pV_F'''+(1-p)V_B'''\right]S^4\end{aligned} \tag{25}$$

Substituting Eq. (25) into Eq. (24), and then the TDGL equation is derived in Eq. (26).

$$\partial_{t1}S=\left\{\partial_{x1}-\frac{pV_F'-(1-p)V_B'+2\lambda\left[pV_F'+(1-p)V_B'\right]}{2(1-rt_d)\left[pV_F'+(1-p)V_B'\right]^2}\partial_{x1}^2\right\}\frac{\delta\Phi(S)}{\delta S} \tag{26}$$

$$\Phi(S)=\int dx_1\left[\frac{pV_F'+(1-p)V_B'+3\lambda b-3b^3t_d^2r\tau}{12}(\partial_{x1}S)^2+\phi(S)\right] \tag{27}$$

where $\delta\Phi(S)/\delta S$ denotes the function derivative. The TDGL, described in Eq. (26), has two steady-state solutions, excluding the trivial solution $S=0$, one is the uniform solution:

$$S(x_1,t_1)=\pm\left\{\frac{12(1-rt_d)\left(-b^2\tau+\frac{1}{2}pV_F'-\frac{1-p}{2}V_B'+\lambda b+r\tau b^2t_d\right)\left[pV_F'+(1-p)V_B'\right]^2}{\left[pV_F'-(1-p)V_B'\right]\left[pV_F'''+(1-p)V_B'''\right]+2\lambda\left[pV_F'+(1-p)V_B'\right]\left[pV_F'''+(1-p)V_B'''\right]}\right\}^{\frac{1}{2}} \tag{28}$$

And the other is the kink solution:

$$\begin{aligned}S(x_1,t_1)=&\pm\left\{\frac{12(1-rt_d)\left(-b^2\tau+\frac{1}{2}pV_F'-\frac{1-p}{2}V_B'+\lambda b+r\tau b^2t_d\right)\left[pV_F'+(1-p)V_B'\right]^2}{\left[pV_F'-(1-p)V_B'\right]\left[pV_F'''+(1-p)V_B'''\right]+2\lambda\left[pV_F'+(1-p)V_B'\right]\left[pV_F'''+(1-p)V_B'''\right]}\right\}^{\frac{1}{2}}\\&\times\tanh\left\{\left[\frac{6b^2\tau-3pV_F'+3(1-p)V_B'-6\lambda b-6r\tau b^2t_d}{pV_F'+(1-p)V_B'+3\lambda b-3b^3t_d^2r\tau}\right]^{\frac{1}{2}}\times(x_1-x_0)\right\}\end{aligned} \tag{29}$$

where x_0 is constant. Eq. (29) represents the coexistence phase.

According to the thermodynamic potential, described in Eq. (25), the coexistence curve, the spinodal line and the critical point can be obtained. The conditions satisfying the coexistence curve are given in Eq. (30).

$$\partial\phi/\partial S = 0, \partial^2\phi/\partial S^2 > 0 \tag{30}$$

The coexistence curve is obtained from Eq. (25) on the basis of the original parameters.

$$(\Delta x)_{co} = h_c \pm \left\{ \frac{12(1-rt_d)\left(-b^2\tau + \frac{1}{2}pV_F' - \frac{1-p}{2}V_B' + \lambda b + r\tau b^2 t_d\right)\left[pV_F' + (1-p)V_B'\right]^2}{\left[pV_F' - (1-p)V_B'\right]\left[pV_F''' + (1-p)V_B'''\right] + 2\lambda\left[pV_F' + (1-p)V_B'\right]\left[pV_F''' + (1-p)V_B'''\right]} \right\}^{\frac{1}{2}} \tag{31}$$

The condition satisfying the spinodal line is given in Eq. (32).

$$\partial^2\phi/\partial S^2 = 0 \tag{32}$$

The spinodal line is obtained from Eq. (25), as shown in the following equation:

$$(\Delta x)_{sp} = h_c \pm \left\{ \frac{4(1-rt_d)\left(-b^2\tau + \frac{1}{2}pV_F' - \frac{1-p}{2}V_B' + \lambda b + r\tau b^2 t_d\right)\left[pV_F' + (1-p)V_B'\right]^2}{\left[pV_F' - (1-p)V_B'\right]\left[pV_F''' + (1-p)V_B'''\right] + 2\lambda\left[pV_F' + (1-p)V_B'\right]\left[pV_F''' + (1-p)V_B'''\right]} \right\}^{\frac{1}{2}} \tag{33}$$

Under the condition $\partial\phi/\partial S = 0$, the critical point is given from Eq. (25).

$$(\Delta x)_c = h_c,\ \tau_c = \frac{pV_F' - (1-p)V_B' + 2\lambda\left[pV_F' + (1-p)V_B'\right]}{2(1-rt_d)\left[pV_F' + (1-p)V_B'\right]^2} \tag{34}$$

5. mKdV equation

Likewise, the slowly varying behavior at long wavelengths near the critical point is researched by deriving the mKdV equation. The slow scales for space variable n and time variable t are also extracted.

Inserting $\alpha_c = \frac{2(1-rt_d)\left[pV_F' + (1-p)V_B'\right]^2}{pV_F' - (1-p)V_B' + 2\lambda\left[pV_F' + (1-p)V_B'\right]}$, $\alpha_c = \left(1+\varepsilon^2\right)\alpha$ into Eq. (21), the following equation is obtained:

$$\varepsilon^4\left[\partial_T R - g_1\partial_X^3 R + g_2\partial_X R^3\right] + \varepsilon^5\left[g_3\partial_X^2 R + g_4\partial_X^4 R + g_5\partial_X^2 R^3\right] = 0 \tag{35}$$

where

$$g_1 = \frac{1}{6}\left(pV_F' + (1-p)V_B'\right) + \frac{1}{2}\lambda b - \frac{1}{2}b^3 t_d^2 r\tau_c \tag{36}$$

$$g_2 = -\frac{1}{6}\left(pV_F''' + (1-p)V_B'''\right) \tag{37}$$

$$g_3 = b^2\tau_c - r\tau_c b^2 t_d \tag{38}$$

$$\begin{aligned} g_4 = {} & \frac{1}{6}(2b\tau_c - \lambda - 2bt_d r\tau_c)\left[pV_F' + (1-p)V_B' + 3\lambda b - 3b^3 t_d^2 r\tau_c\right] \\ & - \frac{1}{24}\left(pV_F' - (1-p)V_B' + 4\lambda b + 4b^4 t_d^3 r\tau_c\right) \end{aligned} \tag{39}$$

$$g_5 = \frac{1}{6}(2b\tau_c - \lambda - 2bt_d r\tau_c)\left(pV_F''' + (1-p)V_B'''\right) - \frac{1}{12}\left[pV_F''' - (1-p)V_B'''\right] \tag{40}$$

where $V_F' = V_F'(h_c) = dV_F(\Delta x_n)/d\Delta x_n|\Delta x_n = h_c$, $V_B' = V_B'(h_c) = dV_B(\Delta x_{n-1})/d\Delta x_{n-1}|\Delta x_{n-1} = h_c$, $V_B''' = V_B'''(h_c) = d^3V_B(\Delta x_{n-1})/d\Delta x_{n-1}^3|\Delta x_{n-1} = h_c$ and $V_F''' = V_F'''(h_c) = d^3V_F(\Delta x_n)/d\Delta x_n^3|\Delta x_n = h_c$.

To obtain the standard mKdV equation, the following transformation is made to Eq. (35):

$$T = \frac{1}{g_1}T',\ R = \sqrt{\frac{g_1}{g_2}}R' \tag{41}$$

Therefore, the regularized mKdV equation, featuring an $O(\varepsilon)$ correction term, is obtained in Eq. (42).

$$\partial_{T'}R' = \partial_X^3 R' - \partial_X R'^3 - \varepsilon\left(\frac{g_3}{g_1}\partial_X^2 R' + \frac{g_4}{g_1}\partial_X^4 R' + \frac{g_5}{g_2}\partial_X^2 R'^3\right) \tag{42}$$

If the term $O(\varepsilon)$ is ignored, the mKdV equation becomes one with the kink solution as the desired solution:

$$R_0'\left(X, T'\right) = \sqrt{c}\tanh\sqrt{\frac{c}{2}}\left(X - cT'\right) \tag{43}$$

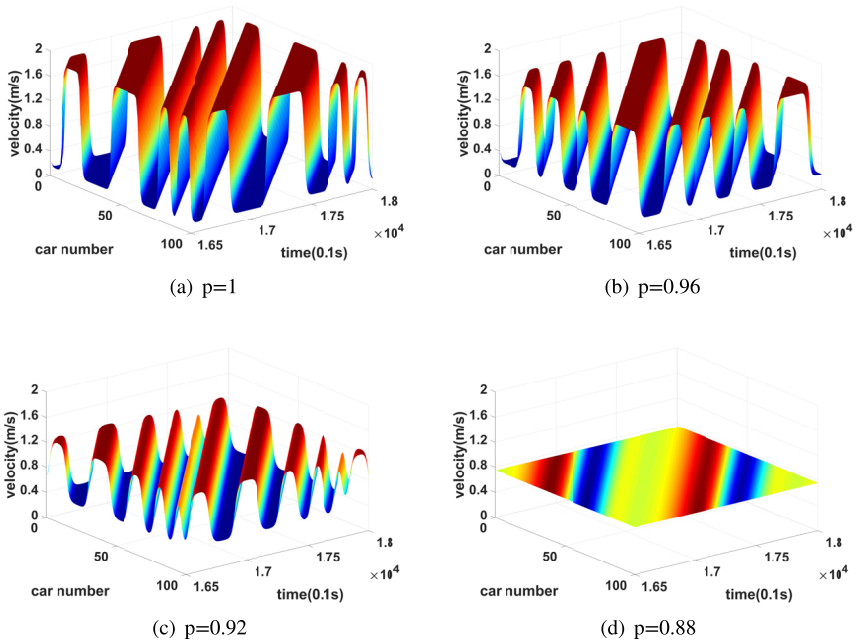

(a) p=1 (b) p=0.96

(c) p=0.92 (d) p=0.88

Fig. 2. Space-time evolution of the velocity after $t = 16500$ time step under different p values.

Following, assuming that $R'(X,T') = R'_0(X,T') + \varepsilon R'_1(X,T')$, the $O(\varepsilon)$ correction term is considered. In order to get the propagation velocity c for the kink solution, $R'_0(X,T')$ must satisfy the solvability condition.

$$\left(R'_0, M\left[R'_0\right]\right) \equiv \int_{-\infty}^{+\infty} dX' R'_0 M\left[R'_0\right] \tag{44}$$

where $M[R'_0] = \frac{g_3}{g_1}\partial_X^2 R' + \frac{g_4}{g_1}\partial_X^4 R' + \frac{g_5}{g_2}\partial_X^2 R'^3$.

The propagation velocity c for the kink solution is obtained.

$$c = \frac{5g_2g_3}{2g_2g_4 - 3g_1g_5} \tag{45}$$

So, the general kink-antikink soliton solution of the headway from the mKdV equation is obtained.

$$\Delta x_n(t) = h_c \pm \sqrt{\frac{g_1 c}{g_2}\left(\frac{\tau}{\tau_c} - 1\right)} \times \tanh\sqrt{\frac{c}{2}\left(\frac{\tau}{\tau_c} - 1\right)} \times \left[n + (1 - cg_1)\left(\frac{\tau}{\tau_c} - 1\right)t\right] \tag{46}$$

Then, the amplitude of the general kink-antikink soliton solution is given in Eq. (47).

$$A = \sqrt{\frac{g_1 c}{g_2}\left(\frac{\tau}{\tau_c} - 1\right)} \tag{47}$$

where $V_F''' < 0, V_B''' < 0$, the general kink-antikink soliton solution also denotes the coexisting phase, which includes the free flow phase which is under low vehicle density and the congested phase which is under high vehicle density. So, the coexistence curves for the free flow phase and the congested phase can be described by $\Delta x_n = h_c + A$ and $\Delta x_n = h_c - A$, as shown by the dotted line in Fig. 1. The kink solution Eq. (46) of the mKdV equation is consistent with the kink solution Eq. (29) of the TDGL equation. Therefore, the jamming transition can be described not only by the TDGL equation with a nontraveling solution, but also by the mKdV equation with a propagating solution.

6. Numerical simulations

In order to verify the accuracy of the theoretical analysis, the TVBL model is simulated numerically. In this study, the periodic boundary conditions are adopted, while the initial conditions are given as follows: the road length $L = 400$ m, the total car number $N = 100$, every time step is 0.1 s, all vehicles are evenly distributed with the same headway distance, and a small disturbance is applied to the head vehicle when the traffic flow is stable, namely

$x_1(0) = L/N + 1$

$x_n(0) = (n-1)L/N (n = 2, 3, \ldots, N)$

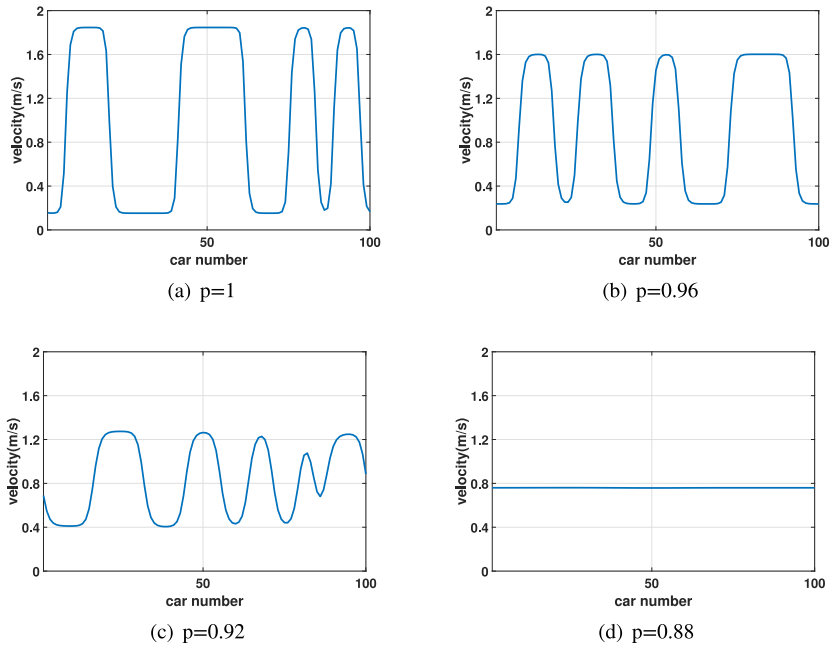

Fig. 3. The velocity profile of each panel, as illustrated in Fig. 2 at $t = 18000$ time step.

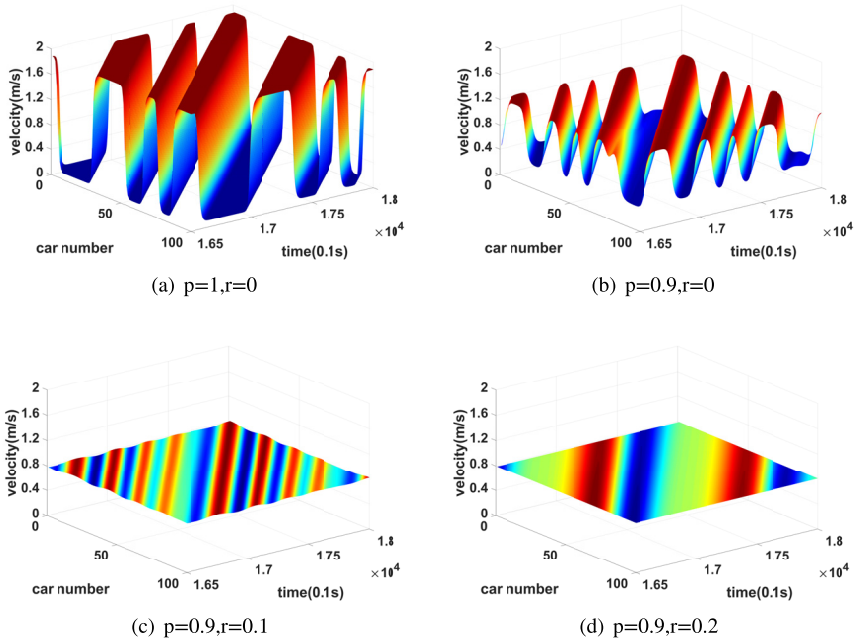

Fig. 4. Space-time evolution of the velocity after $t = 16500$ time step under different values of p and r.

$x'_n(0) = V(L/N)(n = 1, 2, \ldots, N)$ where $\alpha' = 1\ \mathrm{m/s}, \alpha'' = 1\ \mathrm{m/s}, \mathrm{h_c} = 4\ \mathrm{m}, \mathrm{t_d} = 1\ \mathrm{s}$[34,35].

Fig. 2 depicts the space-time evolution diagram of the velocity after $t = 16500$ time step in the case of different parameter p. Other parameters are: $\alpha = 0.85\ \mathrm{s}^{-1}, \lambda = 0.2$ and $r = 0.1\ \mathrm{s}^{-1}$. From pattern (a) to pattern (d) in Fig. 2, the parameter p takes different values, namely $p = 1$, $p = 0.96$, $p = 0.92$ and $p = 0.88$, respectively. It can be clearly shown that the traffic flow is unstable in patterns (a)–(c) and the traffic flow is stable in pattern (d). Specifically, after a small disturbance is applied to the steady traffic flow, as time increases, the small disturbance is continuously amplified, so that the propagating backward stop-and-go traffic jam appears in patterns (a)–(c), whereas this small disturbance disappears in pattern (d). As the value of parameter p increases, the amplitude of the density waves decreases, traffic flow becomes stable and traffic

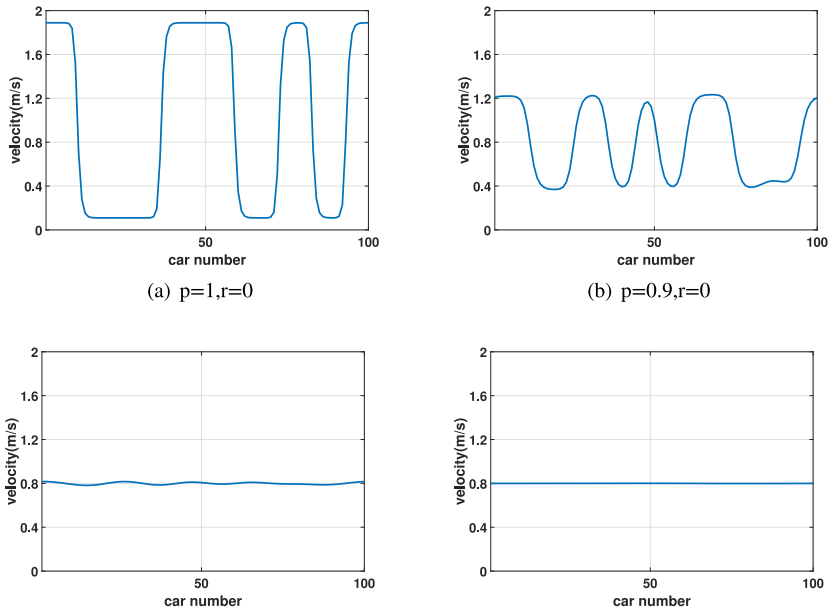

Fig. 5. The velocity profile of each panel, as illustrated in Fig. 4 at $t = 18000$ time step.

jam is alleviated accordingly, especially in pattern (d), where the amplitude of the density waves deteriorates and the traffic flow throughout the space is uniform. This also means that the TVBL model has a general positive impact on traffic flow and more specifically it can make it more stable.

Fig. 3 represents the velocity profile of each panel, as illustrated in Fig. 2 at $t = 18000$ time step. Fig. 3 provides similar results as Fig. 2. As parameter p decreases, the amplitude of the density waves decreases. Traffic congestion is gradually alleviated, and the traffic flow becomes more stable.

Fig. 4 demonstrates the space-time evolution diagram of the velocity after $t = 16,500$ time step in terms of different parameters p and r, where $\alpha = 0.85$ s^{-1} and $\lambda = 0.2$ remain constant. In the case of pattern (a) with $p = 1$ and $r = 0$ s^{-1}, the TVBL model becomes the FVDM. In the case of pattern (b) with $p = 0.9$ and $r = 0$ s^{-1}, the TVBL model becomes the BLVD model. It can be clearly seen that the traffic flow is unstable in pattern (a) and (b), the traffic flow is relatively stable in pattern (c) with $p = 0.9$ and $r = 0.1$ s^{-1}, the traffic flow is stable in pattern (d) with $p = 0.9$ and $r = 0.2$ s^{-1}. When small disturbances are added into the stable traffic flow, as time continues, these are amplified and the traffic jam appears in pattern (a) and (b), while they almost dissipate in pattern (c) and small disturbances totally dissipate in pattern (d). The amplitude of the density waves in pattern (b) is smaller than that in pattern (a). From patterns (b)-(d) in Fig. 4, the amplitude of the density waves gradually becomes weak and the stability is significantly improved for $r = 0, 0.1, 0.2$ s^{-1}, which means that the time-delayed velocity difference considered in this paper has a positive effect on the stability of traffic flow. Hence, as parameter r increases and parameter p decreases, traffic flow becomes more and more stable, which is consistent with the conclusion derived in Fig. 1.

Fig. 5 shows the velocity profile of each panel, as illustrated in Fig. 4 at $t = 18000$ time step. Fig. 5 demonstrates similar results as Fig. 4. Therefore, as parameter p decreases and parameter r increases, traffic flow becomes smoother and more stable.

7. Conclusions and discussion

Based on the FVDM, this paper proposes a modified car-following model by taking into account the time-delayed velocity difference and backward looking effect to analyze traffic behavior and eliminate traffic jams. Through linear stability analysis, the neutral stability curve and critical stability point of the TVBL model are obtained, which clearly shows that the TVBL model can enhance the stability of traffic flow. What's more, the TVBL model is also analyzed through nonlinear method, the TDGL equation describing traffic behavior near the critical stability point has been inferred by making use of the reductive perturbation method. Also, the relationship between the TDGL and the mKdV equations has been demonstrated by establishing the mKdV equation. The results of numerical simulation show that the TVBL model can produce better results, regarding traffic flow stabilization and traffic congestion alleviation, which are in accordance with the conclusions of the theoretical analysis. In the future, in order to enrich and expand the research scope, we will further study the situation that drivers' response delay time obeys various statistical distributions. At the same time, we will also use other possible methodologies such as bifurcation analysis [36], lie group reduction [37] to achieve the objective in relation in this paper.

Declaration of Competing Interest

The authors declare that they have no conflict of interest.

CRediT authorship contribution statement

Guangyi Ma: Conceptualization, Methodology, Software. **Minghui Ma:** Resources, Investigation, Supervision. **Shidong Liang:** Writing - original draft, Formal analysis, Writing - review & editing, Supervision, Data curation. **Yansong Wang:** Data curation, Project administration. **Yaozong Zhang:** Validation, Writing - review & editing.

Acknowledgments

This research was partly funded by Projects of National Natural Science Foundation of China (grant nos. 71801149, 71801153), Technical Service Platform for Vibration and Noise Testing and Control of New Energy Vehicles(Grant No. 18DZ2295900).

References

[1] Cao ZG, Jiang SW, Jie Z, Guo HL. A unified framework for vehicle rerouting and traffic light control to reduce traffic congestion. IEEE Trans Intell Transp Syst 2017;18:1958–73.
[2] Liang SD, Ma MH, He SX, Zhang H, Yuan PC. Coordinated control method to self-equalize bus headways: an analytical method. Transportmetrica B 2019;7:1175–202.
[3] Lu JQ, Wang YQ, Shi XC, Cao JD. Finite-time bipartite consensus for multiagent systems under detail-balanced antagonistic interactions. IEEE Trans Syst Man Cybern -Syst 2019:1–9.
[4] Li ZP, Li WZ, Xu SZ, Qian YQ. Analyses of vehicle's self-stabilizing effect in an extended optimal velocity model by utilizing historical velocity in an environment of intelligent transportation system. Nonlinear Dyn 2015;80:529–40.
[5] Zhai C, Wu WT. A new car-following model considering driver's characteristics and traffic jerk. Nonlinear Dyn 2018;93:2185–99.
[6] Yu GZ, Wang PC, Wu XK, Wang YP. Linear and nonlinear stability analysis of a car-following model considering velocity difference of two adjacent lanes. Nonlinear Dyn 2016;84:387–97.
[7] Li TL, Hui F, Zhao XM. An improved car-following model considering the impact of safety messages. Mod Phys Lett B 2018;32:1850398.
[8] Lárraga ME, JaD R, Alvarez LL. Cellular automata for one-lane traffic flow modeling. Transp Res Pt C 2005;13:63–74.
[9] Ruan X, Zhou JY, Tu HZ, Jin ZR, Shi XF. An improved cellular automaton with axis information for microscopic traffic simulation. Transp Res Pt C 2017;78:63–77.
[10] Cheng RJ, Liu FX, Ge HX. A new continuum model based on full velocity difference model considering traffic jerk effect. Nonlinear Dyn 2017;89:639–49.
[11] Gaddam HK, Meena AK, Rao KR. Kdv-berger solution and local cluster effect of two-sided lateral gap continuum traffic flow model. Int J Mod Phys 2019(B):1950153.
[12] Sun DH, Liu H, Zhang G. A new lattice hydrodynamic model with the consideration of flux change rate effect. Nonlinear Dyn 2018;93:351–8.
[13] Zhang G, Sun DH, Zhao M. Phase transition of a new lattice hydrodynamic model with consideration of on-ramp and off-ramp. Commun Nonlinear Sci Numer Simul 2018;54:347–55.
[14] Bando M, Haseba K, Nakayama A, Shibata A, Sugiyama Y. Dynamical model of traffic congestion and numerical simulation. Phys Rev E 1995;51:1035–42.
[15] Helbing D, Tilch B. Generalized force model of traffic dynamic. Phys Rev E 1998;58:133–8.
[16] Jiang R, Wu QS, Zhu ZJ. Full velocity difference model for a car-following theory. Phys Rev E 2001;64:017101.
[17] Sun DH, Zhang JC, Zhao M. Effect of looking backward and velocity difference in an extended car following model. Sichuan Univ 2012;49:115–20.
[18] Komatsu TS, Sasa S. Kink soliton characterizing traffic congestion. Phys Rev E 1995;52:5574–82.
[19] Nagatani T. Thermodynamic theory for the jamming transition in traffic flow. Phys Rev E 1998;58:4271–6.
[20] Peng G, Lu W, He H, Gu Z. Nonlinear analysis of a new car-following model accounting for the optimal velocity changes with memory. Commun Nonlinear Sci Numer Simul 2016;40:197–205.
[21] Chen C, Cheng RJ, Ge HX. An extended car-following model considering driver's sensory memory and the backward looking effect. Phys A 2019;525:278–89.
[22] Song H, Zheng PJ, Ge HX. TDGL And mkdv equations for an extended car-following model. Nonlinear Dyn 2017;90:2253–62.
[23] Marcinkevicius R, Navickas Z, Ragulskis M, Telksnys T. Solitary solutions to a relativistic two-body problem. Astrophys Space Sci 2016;361:201.
[24] Li ZP, Liu YC. Analysis of stability and density waves of traffic flow model in an ITS environment. Eur Phys J B 2006;53:367–74.
[25] Nagatani T. Density waves in traffic flow. Phys Rev E 2000;61:3564–70.
[26] Zhou J, Shi ZK, Cao JL. Nonlinear analysis of the optimal velocity difference model with reaction-time delay. Phys A 2014;396:77–87.
[27] Chandler RE, Herman R, Montroll EW. Traffic dynamics: studies in car following. Oper Res 1958;6:165–84.
[28] Davis LC. Modifications of the optimal velocity traffic model to include delay due to driver reaction time. Phys A 2003;319:557–67.
[29] Orosz G, Wilson RE, Krauskopf B. Global bifurcation investigation of an optimal velocity traffic model with driver reaction time. Phys Rev E 2004;70:026207.
[30] Orosz G, Krauskopf B, Wilson RE. Bifurcations and multiple traffic jams in a car-following model with reaction-time delay. Phys D 2005;211:277–93.
[31] Yu L, Li T, Shi Z. Density waves in a traffic flow model with reaction-time delay. Phys A 2010;389:2607–16.
[32] Zhou J, Shi ZK, Cao JL. Nonlinear analysis of the optimal velocity difference model with reaction-time delay. Phys A 2014;396:77–87.
[33] Zhang YC, Xue Y, Zhang P, Fan DL, Hong DH. Bifurcation analysis of traffic flow through an improved car-following model considering the time-delayed velocity difference. Phys A 2019;514:133–40.
[34] Green M. "How long does it take to stop?" methodological analysis of driver perception-brake times. TranspHumFact 2000;2:195–216.
[35] Gazis DC, Herman R, Rothery RW. Nonlinear follow-the-leader models of traffic flow. Oper Res 1961;9:545–67.
[36] Orosz G, Krauskopf B, Wilson RE. Bifurcations and multiple traffic jams in a car-following model with reaction-time delay. Phys D 2005;211:277.
[37] Johnpillai AG, Khalique CM. Lie group classification and invariant solutions of mkdv equation with time-dependent coefficients. Commun Nonlinear Sci Numer Simulat 2011;16:1207–15.